Coexistence of Nonvolatile Unipolar Memory and Volatile Threshold Resistance Switching In LaMnO3 Thin Films

yanfeng Yin (yinyf@henu.edu.cn)
Henan University https://orcid.org/0000-0001-6618-412X
ying Zhang
Henan University
caihong Jia
Henan University
weifeng Zhang
Henan University

Nano Express

Keywords: Unipolar resistance switching, Threshold resistance switching, Oxygen vacancies, Insulator-to-metal transition

Posted Date: March 16th, 2020

DOI: https://doi.org/10.21203/rs.3.rs-17337/v1

Coexistence of Nonvolatile Unipolar Memory and Volatile Threshold Resistance Switching In $LaMnO_3$ Thin Films

Yanfeng Yin, Ying Zhang, Caihong Jia[a)] and Weifeng Zhang[a)]

Abstract

Coexistence of nonvolatile unipolar memory and volatile threshold resistive switching was observed in Pt/$LaMnO_3$/Pt system. Specifically, nonvolatile unipolar memory was achieved by applying a negative bias, while volatile threshold resistive switching was obtained at a positive bias. The formation/rupture of conducting filaments and insulator-metal transition are supposed to induce nonvolatile unipolar memory and volatile threshold resistive switching, respectively. The convenient transition between nonvolatile and volatile switching by polarity is very useful for applications in in-memory computing technology.

Keywords: Unipolar resistance switching, Threshold resistance switching, Oxygen vacancies, Insulator-to-metal transition

[a)]Author to whom correspondence should be addressed: chjia@henu.edu.cn and wfzhang@henu.edu.cn. Tel.: +86 371 2388 1940. Fax: +86 371 2388 0659.

Introduction

The resistance switching (RS) can be divided into non-volatile memory resistance switching and volatile threshold resistance switching [1, 2]. In nonvolatile memory RS, both high and low resistance state can be retained under zero bias, which is useful in non-volatile memory devices. In contrast, in volatile threshold RS, only high resistance state (HRS) is stable under zero bias, which hinders its application in nonvolatile memory [2], but its frontier application is in neuromorphic devices [3, 4], novel true random number generators [5] or voltage selectors in resistive random access memories [6, 7]. In perspective of in-memory computing, the cross-point array memories are preferred for the size reduction of bit units, leading to a number of unwanted sneak-path currents [8, 9]. This sneak current can be avoided by using a device with the coexistence of unipolar memory and threshold resistance switching.

$LaMnO_3$ (LMO) compound as a Mott insulator and an A-type antiferromagnetic insulating material (with ferromagnetic spin correlations on a (001) crystal plane and antiferromagnetism between these crystal planes) [10] has been widely studied due to resistive switching characteristics by controlling oxygen content or electronic reconstruction [11, 12]. The mutually transition between the nonvolatile unipolar memory switching and volatile threshold switching have been achieved by measurement temperature [13], oxygen content [1], compliance current [14], and electrical pulse polarity [15]. In our present work, we report on the transition between nonvolatile unipolar memory and volatile threshold RS in a simple $LaMnO_3$ thin film at room temperature by dc voltage polarity. The nonvolatile unipolar memory

switching and the volatile threshold switching may originate from the opposite migration direction of oxygen vacancies under different voltage polarity. For many actual applications, endurance is a key parameter. TaO_x [16] and VO_2 [17] have endurance of over 10^{10} cycles as nonvolatile and volatile memory, respectively, but only over 100 cycles when nonvolatile memory and volatile threshold switching coexist [18, 19]. In the present work, $LaMnO_3$ exhibits a stable threshold switching over 1000 cycles and unipolar memory switching over 500 cycles on the same device, and the convenient voltage polarity control mode are very useful for applications in in-memory computing technology.

Methods

Polycrystalline $LaMnO_3$ films were deposited on $Pt/Ti/TiO_2/SiO_2/Si$ substrate by pulsed laser deposition (PLD) using a KrF excimer laser (248 nm, 25 ns pulse duration, COMPexPro201, Coherent) at an energy of 300 mJ and frequency of 5 Hz, with the base vacuum of 2×10^{-4} Pa. During deposition, the substrate temperature was kept at 750 ℃, and the target-substrate distance was 6.5 cm. The oxygen partial pressure was 5×10^{-4} Pa, and the growth time was 20 min. After growth, the sample was annealed in situ for 20 min, and then, the temperature was reduced to room temperature at 10 ℃/min within a vacuum environment. In order to measure electrical properties, top electrode Pt (0.04 mm^2) were sputtered on $LaMnO_3$ thin films through a shadow mask by DC sputtering at room temperature. Then, the sample was again annealed in PLD chamber, at 500 ℃ under 5×10^{-4} Pa oxygen pressure for 30 min. The x-ray diffraction (XRD, DX-2700) was used to measure the structure of LMO film.

The atomic force microscope (AFM) and scanning electron microscope (SEM) were employed to characterize the surface morphology and cross-section image of film by Burke Multimode 8 and JSM-7001F instrument, respectively. Electrical properties were measured using Keithley 2400 source meter, the corresponding structure of our device is shown in the inset of Fig. 1a.

Results and Discussion

From XRD patterns shown in Fig. 1a, the LMO film was polycrystalline on Pt/Ti/TiO_2/SiO_2/Si substrate. From the atomic force microscope image shown in Fig. 1b, the LMO film is granular and uniform. The thickness is around 140 nm from the cross sectional SEM image shown in Fig. 1c. On the same Pt/$LaMnO_3$/Pt device unit, the nonvolatile unipolar memory switching and volatile threshold switching can be controlled by applying the different polarities of sweep voltage. Figure 1d presents the initial positive reset I-V curve of Pt/$LaMnO_3$/Pt devices. It can be seen that the pristine resistance state of Pt/$LaMnO_3$/Pt device is at low resistance state (LRS), as shown in the upper left inset of Fig. 1d. When the positive sweep voltage increases from 0 V to about 3 V, a sudden decrease in current at the first scanning occurs and a slightly higher resistance is achieved, but this is not a stable resistive state. While sweeping back to a lower voltage close to 2 V, a sharp drop of current appears, a high resistance is obtained. After that, if a positive sweep voltage is applied again, the volatile threshold switching emerges, as shown in the Fig. 2a. Although the device is switched to a low resistance at a threshold voltage (V_{th}) of around 3.40 V (on-switching), it spontaneously goes back to the HRS at a low voltage (V_{hold}) about

2.35 V (self-off-switching). This means that the LRS is unable to maintain in the volatile threshold switching material. In order to protect the device from hard breakdown, a compliance current of 0.002 A was adopted in the test. After the above process, the $LaMnO_3$ film exhibits a repeatable threshold switching behavior in continuous forward DC sweeping measurements. Here, the threshold switching of 1000 cycles are measured on the same device unit. The statistical distribution of the V_{th} and V_{hold} with the number of cycles and the Lorentz fitting of V_{th} is shown in the Fig. 2b, As can be seen from the fitting results, the threshold voltage is (3.40±0.40) V, the corresponding electric field is $(2.43 \pm 0.29)\times10^5$ V/cm, which is comparable with previous reports [5, 6]. Figure 2c shows the cumulative distributions of V_{th} and V_{hold}, the on-switching voltages (V_{th}) vary within the 0.50 V range, but the self-off-switching voltages (V_{hold}) are almost stable at 2.35 V, the variations of the V_{th} and V_{hold} is similar to that of VO_2 [6]. The V_{th} and V_{hold} change with the threshold switching cycles in Fig. 2d, the threshold voltages decrease as the number of cycles increases, however, there is no such change in the self-off-switching voltages. That is, the V_{hold} is more stable than V_{th} in the threshold switching, which has also been observed in other Mott two-terminal devices, such as VO_2 [6].

It is worth noting that the volatile threshold switching under a forward voltage is converted into nonvolatile unipolar memory switching by applying a reverse voltage. Figure 3a shows 500 unipolar switching cycles obtained on the same device, by sweeping the voltage from zero to a negative value, a low current is achieved, the current increases abruptly and it turns back to a low resistance (on state) at a certain

voltage (set voltage V_{set}), during this time, a compliance current was used to avoid the dielectric breakdown of the $LaMnO_3$ film layer. While sweeping the negative voltage again, originally, a high current is measured, but the current suddenly drops to the initial value (off state) at a certain voltage (reset voltage V_{reset}), the reset voltage is much lower than set voltage. The statistical distribution and corresponding Lorentz fitting results of the V_{set} and V_{reset} are shown in the Fig. 3b, the set and reset voltages are -7.46 ± 3.26 V and -2.65 ± 1.85 V, respectively, the corresponding electric field (10^5 V/cm) is lower than that of memory resistance switching Ni/NiO core-shell nanowires (10^6 V/cm), which is helpful for reducing the energy consumption in memory devices [2]. Figure 3c shows the cumulative distributions of the V_{set} and V_{reset}, a slightly wider distribution of the V_{set} and V_{reset} than that in memory resistance switching Ni/NiO core-shell nanowires, which might be caused by more measurement cycles of Pt/$LaMnO_3$/Pt device, while there is only about 25 cycles of Ni/NiO core-shell nanowires [2]. The resistance values of the HRS and LRS were on the order of 10^4 Ω and about 60 Ω, respectively, as shown in Fig. 3d, and the R_{OFF}/R_{ON} ratio is close to 10^3. By applying the forward voltage again, the $LaMnO_3$ film recovers to reproducible threshold switching behaviors after setting unipolar memory switching to the HRS.

As stated above, the $LaMnO_3$ film was fabricated and annealed under a low oxygen pressure (5×10^{-4} Pa), so there are a large amount of oxygen vacancies, which has been confirmed by synchrotron-based X-ray diffraction (SXRD) and aberration-corrected scanning transmission electron microscopy (STEM) [11].

Meanwhile, the rectification characteristics in the lower right inset in Fig. 1d suggests that the top Pt/$LaMnO_3$ interface is responsible for the resistance switching. Due to the presence of oxygen vacancies, a pristine low resistance state has been obtained in our device. As it is known that the oxygen-deficient LMO is generally considered as an n-type semiconductor, because the oxygen vacancies act as donors in oxides and become positively charged after releasing electrons to the conduction band [11, 20]. Furthermore, based on the rectification direction, as shown in the lower right inset of Fig. 1d, the bottom electrode interface can be seen as an ohmic-like contact, and top electrode interface can be treated as an Schottky-like contact. Thus we can attribute both the threshold and unipolar switching to the top electrode interface. Figure 4a shows the schematic band structure of the HRS of Pt/LMO/Pt after applying a forward bias. Under a positive bias, the oxygen vacancies drift away from the top electrode interface, which results in a wider and higher barrier at the top Pt/LMO interface, leading to a LRS to HRS transition [11]. Meanwhile, and the concentration of oxygen vacancies in bulk $LaMnO_3$ films enhances accompanied with the oxygen vacancies drifting into the bulk. It is well known that in the stoichiometric $LaMnO_3$, the oxidation state of Mn is +3 [21, 22]. When there are a lot of oxygen vacancies in $LaMnO_3$ film, charge disproportionation effect of the $Mn^{3+} \rightarrow Mn^{2+}$ possibly happens, and the concentration enhancement of oxygen vacancies will lead to an increase of Mn^{2+} concentration [21]. Then the double exchange (DE) effect occurs in Mn^{2+}-O-Mn^{3+} in our oxygen-deficient $LaMnO_3$ electron-doped films, just as in the case in Mn^{3+}-O-Mn^{4+} in the hole-doped manganites [21, 23]. Thus the ferromagnetic

metal phase increases due to the enhancement of double exchange effect between the Mn^{2+} and Mn^{3+}, which is unevenly distributed in the charge ordered antiferromagnetic insulator phase of $LaMnO_3$ film [23]. Furthermore, the resistivity of the ferromagnetic state is much larger than that of ordinary metals, which may be caused by electrons localization from magnetic disorder [24]. Accordingly, an intermediate resistance state appears during the initial positive reset transition in our Pt/$LaMnO_3$/Pt device, as shown in Fig. 1d. In the present oxygen-deficient bulk LMO films, more ferromagnetic metal clusters phase coexist with antiferromagnetic insulating phase. The intermediate resistance state is higher than the initial low resistance state, which is called bad metallic state [25]. When applying a positive bias, a percolation type transition between the insulating phase and bad metallic phase plays a major role, as shown in the schematic diagram of Fig. 4b, c, so the insulator-metal transition occurs, and the device shows the characteristics of threshold switching with a comparable threshold electric field of VO_2 [23]. The schematic band structure of Pt/LMO/Pt at LRS after a negative bias is shown in Fig. 4d. Under a negative bias, the oxygen vacancies drift toward the top electrode interface, leading to a decrease in the height and width of the Schottky barrier and the device is set to the LRS of the unipolar memory switching. Simultaneously, the concentration of oxygen vacancies in bulk $LaMnO_3$ films reduces, and the ratio of Mn^{2+}/Mn^{3+} decreases in the bulk $LaMnO_3$ film, the concentration of ferromagnetic metal phase reduces due to the reduction of the double exchange effect between the Mn^{2+} and Mn^{3+}, so the formation and fracture of oxygen vacancies conducting filaments should be responsible for the unipolar

switching. The oxygen vacancies conducting channel between the top and bottom electrodes will be formed under negative bias, as can be seen from the Fig. 4e, f, when the negative bias is applied again, the oxygen vacancies conductive filaments is disconnected with the help of Joule heating, and the device switches from the low resistance state to the high resistance state.

Conclusions

In summary, coexistence of the nonvolatile unipolar memory and volatile threshold resistance switching was observed in $LaMnO_3$ film, which is dependent on the bias polarity. The voltage polarity affects the migration direction/distribution of oxygen vacancies and the width/height of the top interface barrier, resulting in a transition between nonvolatile unipolar switching and volatile threshold switching. Because of its excellent endurance, our device is expected to be used in in-memory computing technology and accelerate the development of post-Moore industry.

Abbreviations

RS: Resistance switching; LMO: $LaMnO_3$; PLD: Pulsed laser deposition;

XRD: X-ray diffraction; AFM: Atomic force microscope; SEM: Scanning electron microscope; HRS: High-resistance state; LRS: Low-resistance state; V_{th}: threshold voltage; V_{set}: set voltage; V_{reset}: reset voltage; DE: double exchange;

Funding

This work was supported by the National Natural Science Foundation of China (11974099).

Availability of Data and Materials

All the data and materials are available by contacting the corresponding author.

Authors' Contributions

YY carried out the experimental design, the growth and measurement. YZ participated in the measurement. CJ participated in the experimental analysis and revised the manuscript. WZ supervised the research. All authors read and approved the final manuscript.

Competing Interests

The authors declare that they have no competing interests.

Acknowledgements

Not Applicable.

Author details

Henan Key Laboratory of Photovoltaic Materials, Laboratory of Low-Dimensional Materials Science, Henan University, Kaifeng 475004, People's Republic of China

REFERENCES

1. Seo S, Lee MJ, Seo DH, Jeoung EJ, Suh DS, Joung YS, Yoo IK, Hwang IR, Kim SH, Byun IS, Kim JS, Choi JS, Park BH (2004) Reproducible resistance switching in polycrystalline NiO films. Appl Phys Lett 85:5655-5657
2. He L, Liao ZM, Wu HC, Tian XX, Xu DS, Cross GLW, Duesberg GS, Shvets IV, Yu DP (2011) Memory and threshold resistance switching in Ni/NiO core-shell nanowires. Nano Lett 11:4601-4606
3. Pickett MD, Medeiros-Ribeiro G, Williams RS (2012) A scalable neuristor built with Mott memristors. Nat Mater 12:114-117
4. Valle JD, Salev P, Tesler F, Vargas NM, Kalcheim Y, Wang P, Trastoy J, Lee MH, Kassabian G, Ramírez JG, Rozenberg MJ, Schuller IK (2019) Subthreshold firing in Mott nanodevices. Nature 569:388-392
5. Jiang H, Belkin D, Savel'ev SE, Lin SY, Wang ZR, Li YN, Joshi S, Midya R, Li C, Rao MY, Barnell M, Wu Q, Yang JJ, Xia QF (2017) A novel true random number generator based on a stochastic diffusive memristor. Nat. Commun 8:882
6. Zhou Y, Ramanathan S (2015) Mott memory and neuromorphic devices. Proc IEEE 103:1289-1310
7. Yang JJ, Zhang MX, Pickett MD, Miao F, Strachan JP, Li WD, Yi W, Ohlberg DAA, Choi BJ, Wu W, Nickel JH, Medeiros-Ribeiro G, Williams RS (2012) Engineering nonlinearity into memristors for passive crossbar applications. Appl Phys Lett 100:113501
8. Ielmini D, Wong H-SP (2018) In-memory computing with resistive switching devices. Nature Electronics 1:333
9. Gao L, Chen PY, Liu R, Yu S (2016) Physical unclonable function exploiting sneak paths in resistive cross-point array. IEEE Trans Electron Devices 63:3109-3115
10. Dagotto E, Hotta T, Moreo A (2001) Colossal magnetoresistant materials: the key role of phase separation. Phys Rep 344:1
11. Xu ZT, Jin KJ, Gu L, Jin YL, Ge C, Wang C, Guo HZ, Lu HB, Zhao RQ, Yang GZ (2012) Evidence for a crucial role played by oxygen vacancies in $LaMnO_3$ resistive switching memories. Small 8:1279-1284
12. Huang XH, Xu M, Xu ZX, Yan JM, Zheng RK (2019) Electric-field tuning of nonvolatile resistance change and magnetic properties of $LaMnO_3$/PMN-PT(011) heterostructure. Materials Letters 254:89-91
13. Chang SH, Lee JS, Chae SC, Lee SB, Liu C, Kahng B, Kim DW, Noh TW (2009) Occurrence of both unipolar memory and threshold resistance switching in a NiO film. Phys Rev Lett 102: 026801
14. Peng HY, Li YF, Lin WN, Wang YZ, Gao XY, Wu T (2012) Deterministic conversion between memory and threshold resistive switching via tuning the strong electron correlation. Sci Rep 2:442
15. Hwang I, Lee MJ, Buh GH, Bae J, Choi J, Kim JS, Hong S, Kim YS, Byun IS, Lee SW, Ahn

SE, Kang BS, Kang SO, Park BH (2010) Resistive switching transition induced by a voltage pulse in a Pt/NiO/Pt structure. Appl Phys Lett 97:052106

16. Lee MJ, Lee CB, Lee D, Lee SR, Chang M, Hur JH, Kim YB, Kim CJ, Seo DH, Seo S, Chung UI, Yoo IK, Kim K (2011) A fast, high-endurance and scalable non-volatile memory device made from asymmetric Ta_2O_{5-x}/TaO_{2-x} bilayer structures. Nat Mater 10:625-630
17. Radu IP, Govoreanu B, Martens K, Toeller M, Peter AP, Ikram MR, Zhang L, Hody H, Kim W, Favia P, Conard T, Chou HY, Put B, Afanasiev V, Stesmans A, Heyns M, Gendt SD, Jurczak M (2013) Vanadium Dioxide for Selector Applications. ECS Trans 58:249
18. Son M, Liu XJ, Sadaf SM, Lee D, Park S, Lee W, Kim S, Park J, Shin J, Jung S, Ham MH, Hwang H (2012) Self-selective characteristics of nanoscale VO_x devices for high-density ReRAM applications. IEEE Electron Device Lett 33:5
19. Sharath SU, Joseph MJ, Vogel S, Hildebrandt E, Komissinskiy P, Kurian J, Schroeder T, Alff L (2016) Impact of oxygen stoichiometry on electroforming and multiple switching modes in TiN/TaO_x/Pt based ReRAM. Appl Phys Lett 109:173503
20. Basu SR, Martin LW, Chu YH, Gajek M, Ramesh R, Rai RC, Xu X, Musfeldt JL (2008) Photoconductivity in $BiFeO_3$ thin films. Appl Phys Lett 92:091905
21. Zhao RQ, Jin KJ, Xu ZT, Guo HZ, Wang L, Ge C, Lu HB, Yang GZ (2013) The oxygen vacancy effect on the magnetic property of the $LaMnO_{3-\delta}$ thin films. Appl Phys Lett 102:122402
22. Abbate M, Groot de FMF, Fuggle JC, Fujimori A, Strebel O, Lopez F, Domke M, Kaindl G, Sawatzky GA, Takano M, Takeda Y, Eisaki H, Uchida S (1992) Controlled-valence properties of $La_{1-x}Sr_xFeO_3$ and $La_{1-x}Sr_xMnO_3$ studied by soft-x-ray absorption spectroscopy. Phys Rev B 46:4511
23. Peng JJ, Song C, Cui B, Li F, Mao HJ, Wang YY, Wang GY, Pan F (2014) Exchange bias in a single $LaMnO_3$ film induced by vertical electronic phase separation. Phys Rev B 89: 165129
24. Lu WJ, Sun YP, Zhao BC, Zhu XB, Song WH (2006) Induced ferromagnetism in Mo-substituted $LaMnO_3$. Phys Rev B 73:174425
25. Nath R, Raychaudhuri AK, Mukovskii YM, Andreev N, Chichkov V (2014) Room temperature resistive state switching with hysteresis in $GdMnO_3$ thin film with low threshold voltage. Appl Phys Lett 104:183508

Figure of captions

Fig. 1 a XRD pattern of LMO film, the inset shows the structure diagram of the device. **b** The atomic force microscope image of the LMO film. **c** Cross-sectional SEM image of the LMO film deposited on Pt/Ti/SiO_2/Si substrate. **d** The initial positive reset I-V curves of Pt/$LaMnO_3$/Pt device, the upper left and lower right insets show the low resistance state and high resistance state I-V curves measured over ±2 V range, respectively.

Fig. 2 a 1000 consecutive positive bias volatile threshold switching cycles. **b** The statistical distribution of the V_{th} and V_{hold} with the number of cycles, the black solid line corresponds to a Lorentz fit curve of V_{th}. **c** The cumulative distribution of the V_{th} and V_{hold}. **d** The V_{th} and V_{hold} as a function of the number of cycles.

Fig. 3 a 500 cycles of nonvolatile negative bias unipolar switching. **b** Statistical distribution of V_{set} and V_{reset} with the number of cycles, the red and black solid lines are corresponding to the Lorentz fit curves. **c** The cumulative distribution of the V_{set} and V_{reset}. **d** Endurance test of LRS and HRS obtained with a reading voltage of -0.3 V.

Fig. 4 The schematic energy band structure of initial positive high resistance state and negative low resistance state (**a, d**), The schematic diagram of the threshold switching (**b, c**) and the unipolar switching (**e, f**). In diagram, the "plus" and "minus" symbols represent positive and negative polarity of voltage, respectively. The "circled plus" symbols represent the ionized oxygen vacancies. The dark arrows show the drifting direction of the ionized oxygen vacancies. The "hollow circle" symbols represent the oxygen vacancies. In (**b**)、(**c**)、(**e**) and (**f**), the schematic distribution of metallic (black) and insulating (light blue) domains; the orange and black line represent the top and bottom Pt electrode, respectively.

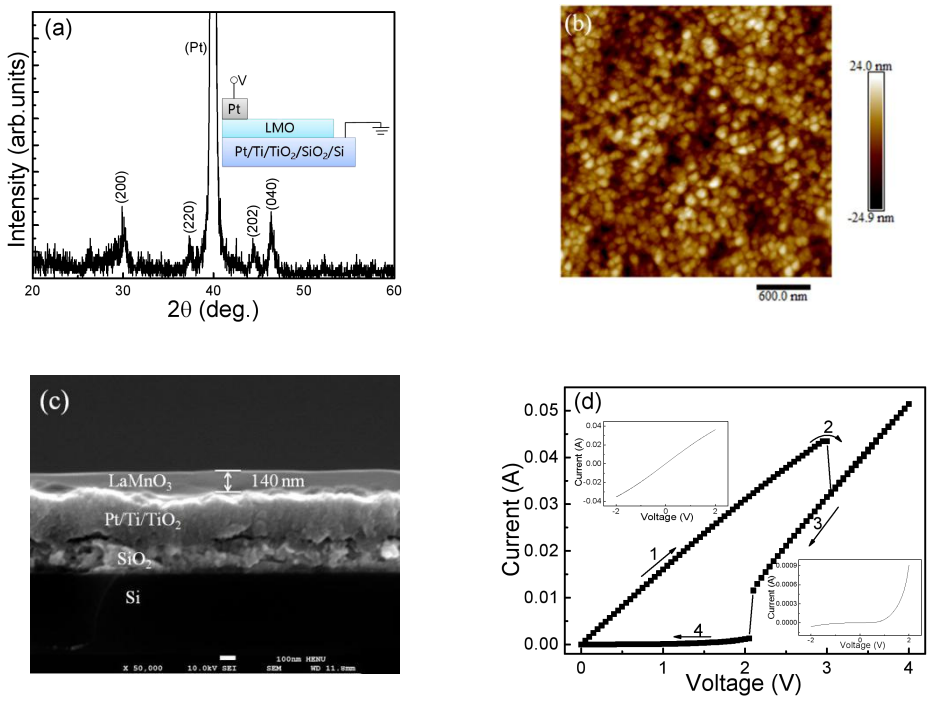
(a)
(Pt)
V
Pt
LMO
Pt/Ti/TiO2/SiO2/Si
(200)
(220)
(202)
(040)
Intensity (arb.units)
20
30
40
50
60
2θ (deg.)
(b)
24.0 nm
-24.9 nm
600.0 nm
(c)
LaMnO3
140 nm
Pt/Ti/TiO2
SiO2
Si
(d)
Current (A)
Voltage (V)
1
2
3
4

Fig. 1

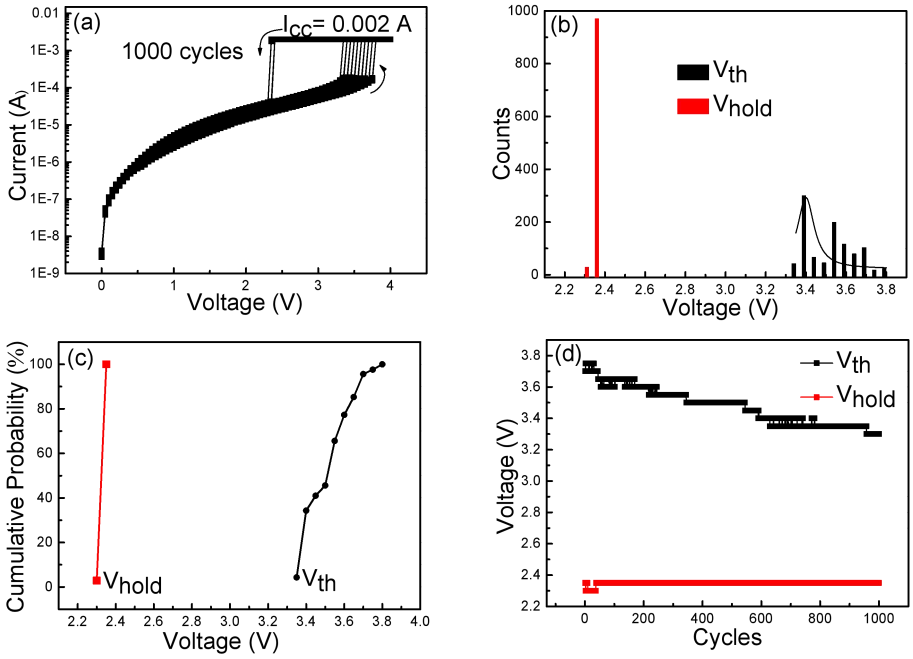
(a)
1000 cycles
I_{cc}= 0.002 A
Current (A)
Voltage (V)
(b)
V_{th}
V_{hold}
Counts
Voltage (V)
(c)
V_{hold}
V_{th}
Cumulative Probability (%)
Voltage (V)
(d)
V_{th}
V_{hold}
Voltage (V)
Cycles

Fig. 2

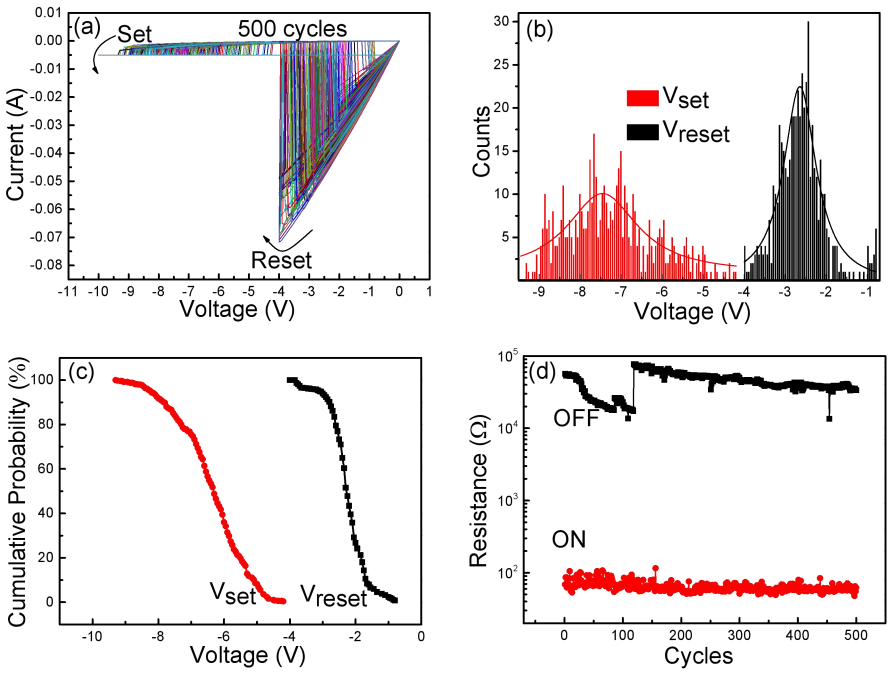
(a)
Set
500 cycles
Reset
Current (A)
Voltage (V)
(b)
Vset
Vreset
Counts
Voltage (V)
(c)
Vset
Vreset
Cumulative Probability (%)
Voltage (V)
(d)
OFF
ON
Resistance (Ω)
Cycles

Fig. 3

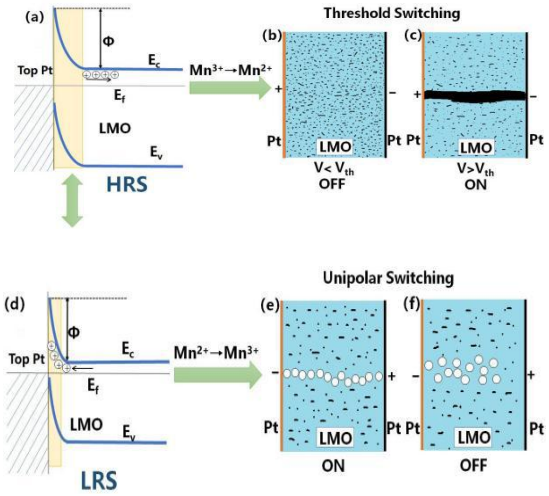
(a)
Φ
E_c
Top Pt
E_f
LMO
E_v
HRS
$Mn^{3+} \rightarrow Mn^{2+}$
Threshold Switching
(b)
(c)
Pt
LMO
Pt Pt
LMO
Pt
$V < V_{th}$
OFF
$V > V_{th}$
ON
(d)
Φ
E_c
Top Pt
E_f
LMO
E_v
LRS
$Mn^{2+} \rightarrow Mn^{3+}$
Unipolar Switching
(e)
(f)
Pt
LMO
Pt Pt
LMO
Pt
ON
OFF

Fig. 4

Figures

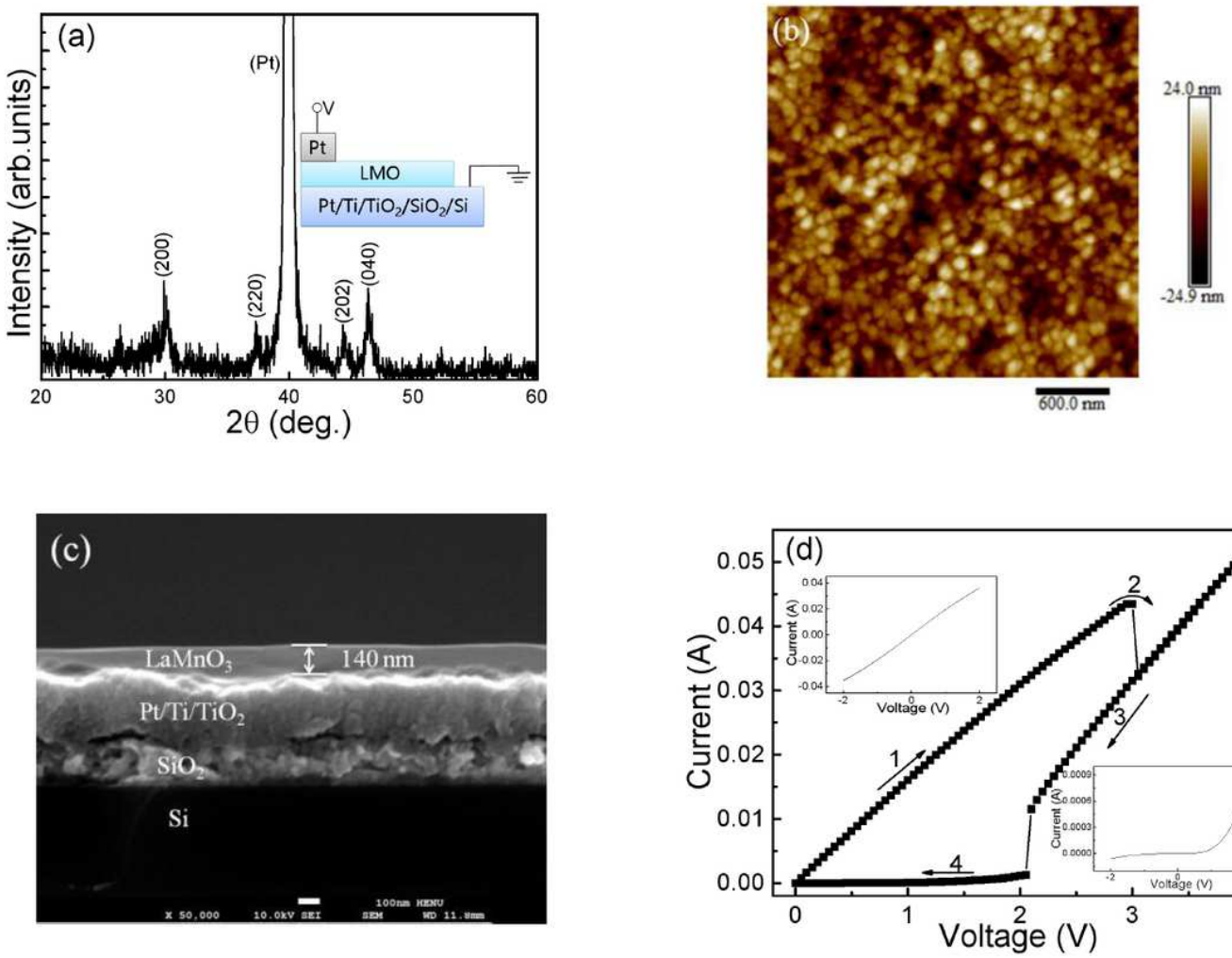

Figure 1

a XRD pattern of LMO film, the inset shows the structure diagram of the device. b The atomic force microscope image of the LMO film. c Cross-sectional SEM image of the LMO film deposited on Pt/Ti/SiO2/Si substrate. d The initial positive reset I-V curves of Pt/LaMnO3/Pt device, the upper left and lower right insets show the low resistance state and high resistance state I-V curves measured over ±2 V range, respectively.

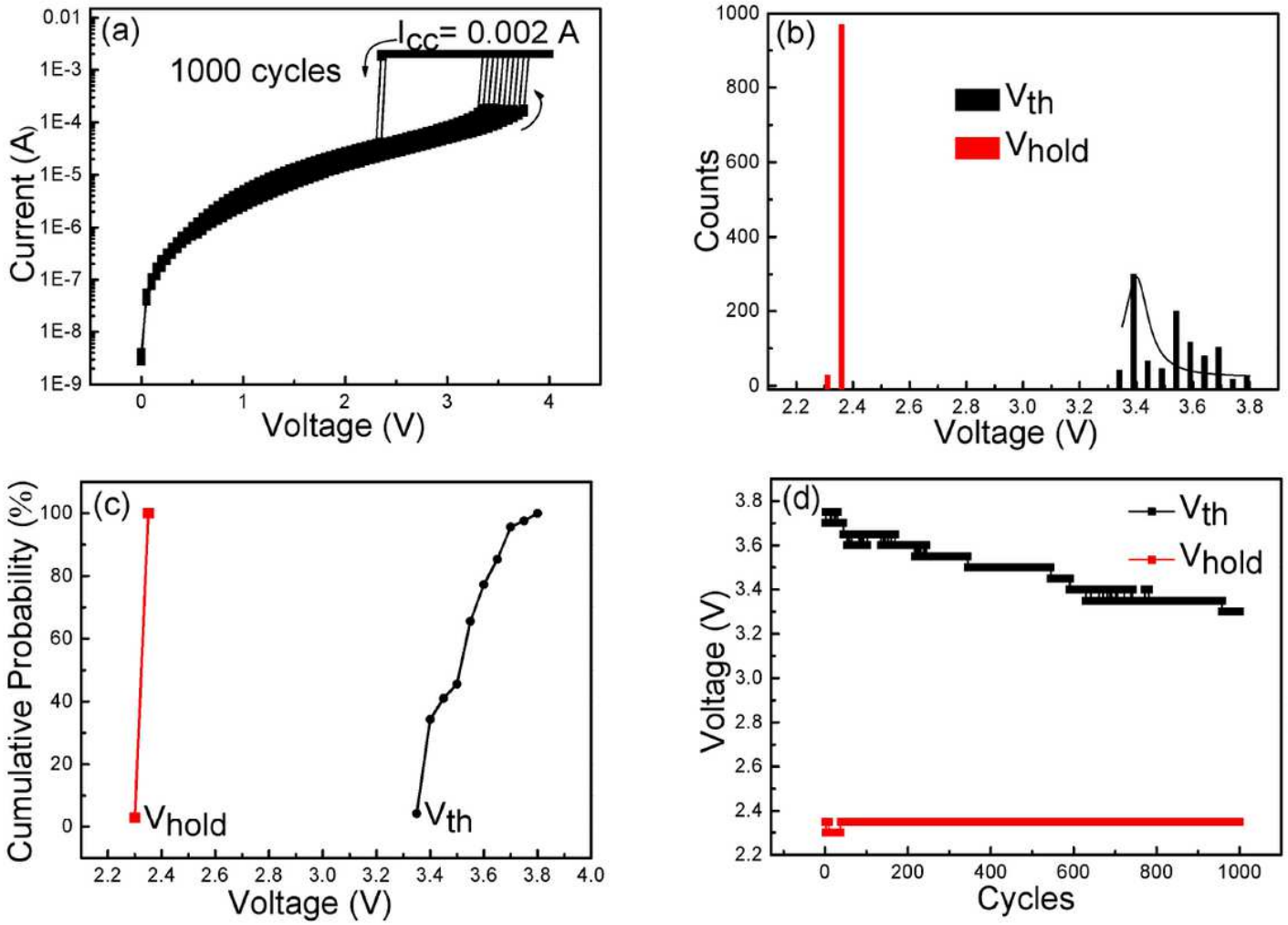

Figure 2

a 1000 consecutive positive bias volatile threshold switching cycles. b The statistical distribution of the Vth and Vhold with the number of cycles, the black solid line corresponds to a Lorentz fit curve of Vth. c The cumulative distribution of the Vth and Vhold. d The Vth and Vhold as a function of the number of cycles.

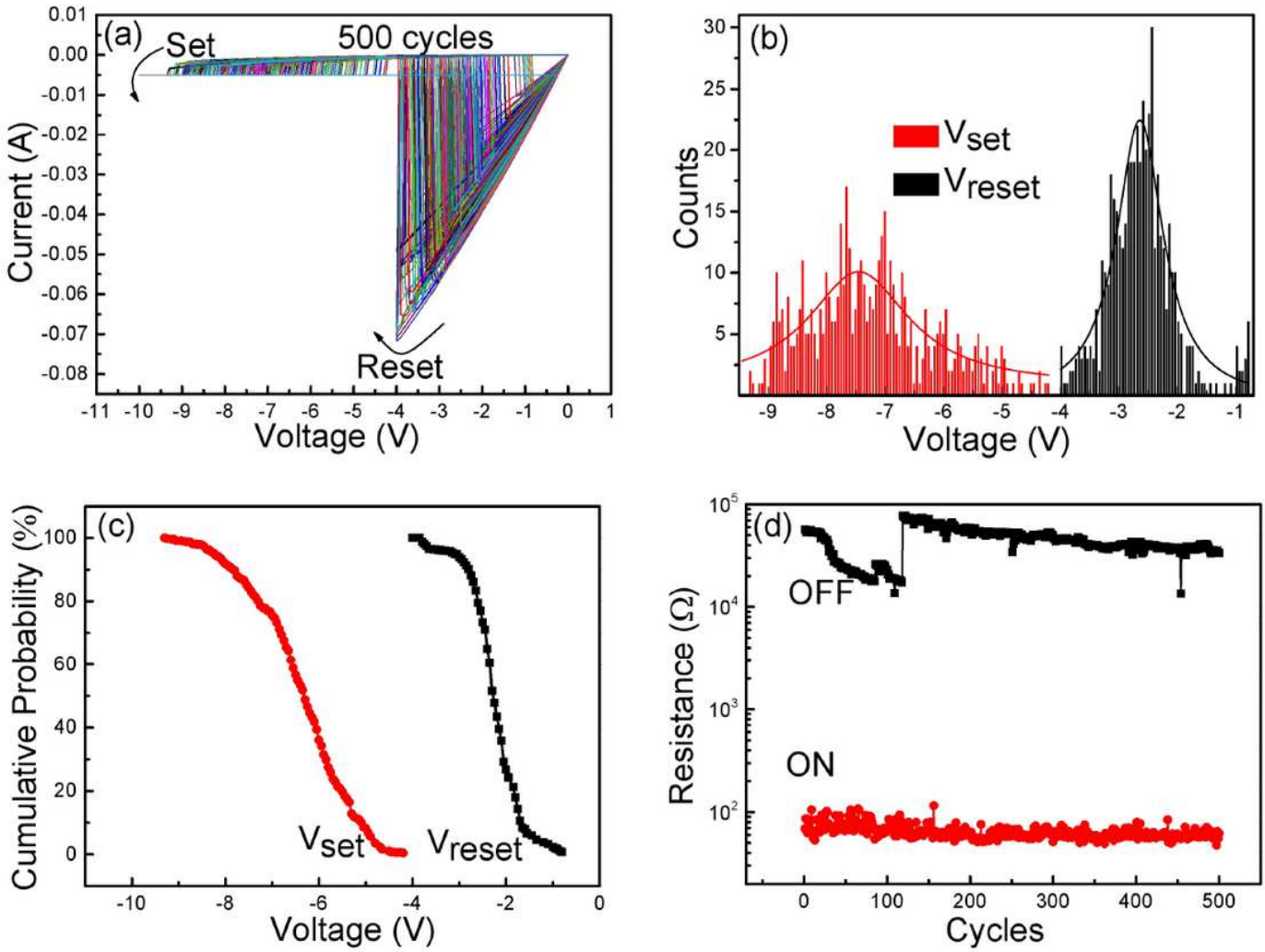

Figure 3

a 500 cycles of nonvolatile negative bias unipolar switching. b Statistical distribution of Vset and Vreset with the number of cycles, the red and black solid lines are corresponding to the Lorentz fit curves. c The cumulative distribution of the Vset and Vreset. d Endurance test of LRS and HRS obtained with a reading voltage of -0.3 V.

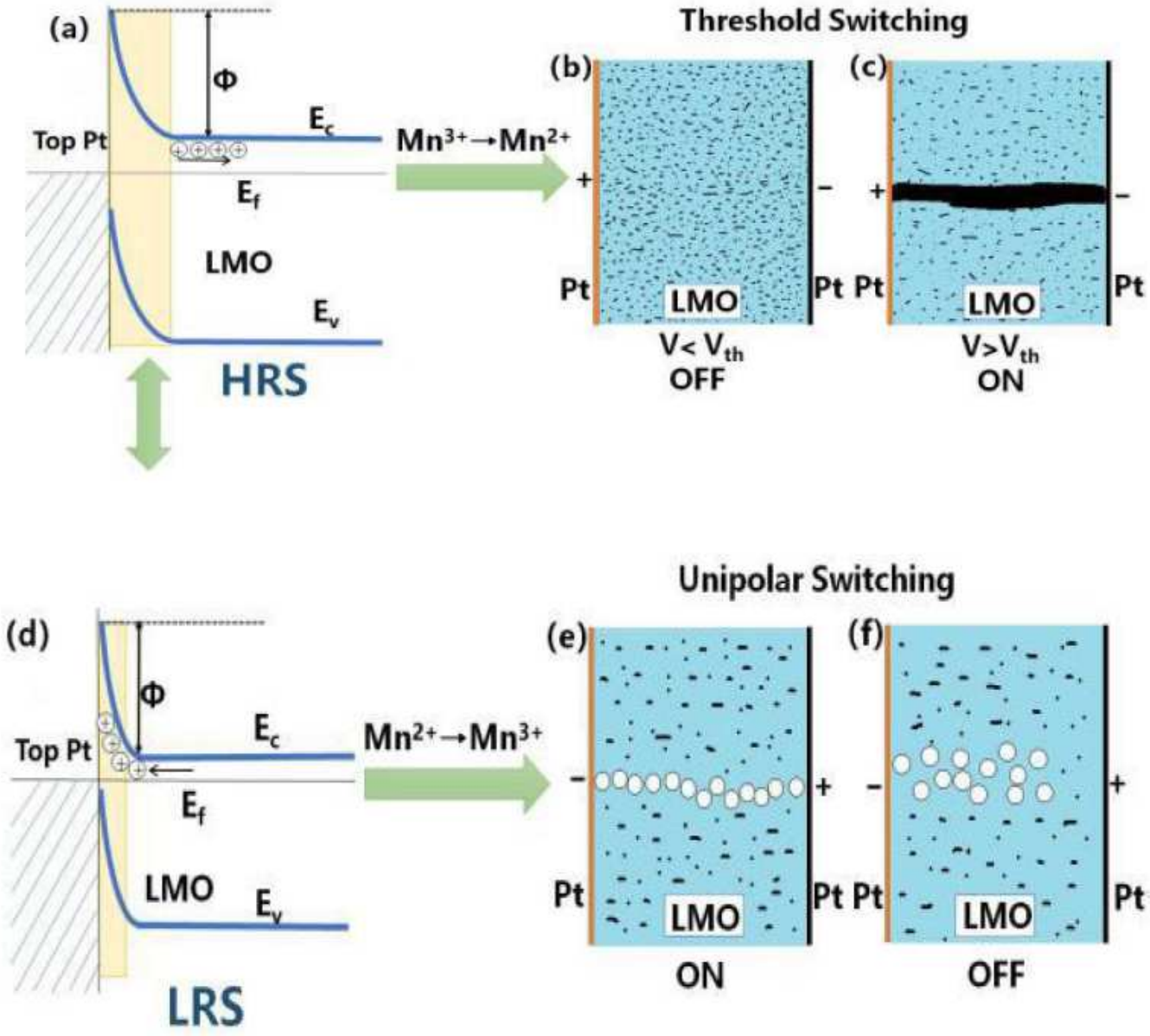

Figure 4

The schematic energy band structure of initial positive high resistance state and negative low resistance state (a, d), The schematic diagram of the threshold switching (b, c) and the unipolar switching (e, f). In diagram, the “plus” and “minus” symbols represent positive and negative polarity of voltage, respectively. The “circled plus” symbols represent the ionized oxygen vacancies. The dark arrows show the drifting direction of the ionized oxygen vacancies. The “hollow circle” symbols represent the oxygen vacancies. In (b)、(c)、(e) and (f), the schematic distribution of metallic (black) and insulating (light blue) domains; the orange and black line represent the top and bottom Pt electrode, respectively.